BUTTERWORTH HEINEMANN

Composites **26** (1995) 757–765

0010-4361/95/$10.00

Bending failure of aramid fibre-reinforced composite

S. L. Bazhenov
Institute of Chemical Physics, Russian Academy of Science, Kosygin Street 4, 117 977 Moscow, Russia
(Received 21 March 1995)

Flexural failure of a unidirectional aramid SVM/epoxy composite was studied using two-point loading of half-ring specimens. Failure originated near the compressive side of the specimen where several intersecting shear yield bands, similar to slip bands in metals, were observed. The angle between the yield bands and the loading direction was 45 ± 2°. The thickness of the yield bands grew proportionally to the shear displacement of their opposite sides. The yield stress of the SVM fibres in bending was equal to 500 MPa, which is close to the fibre strength in pure axial compression of 400–450 MPa. The maximum failure stress of the composite in bending, 530 MPa, was approximately twice as high as the strength of the composite under pure axial compression (260–280 MPa). In bending the composite is elastic in the tensile part of the beam whilst the other, compressed, part is elastic-plastic.

(Keywords: aramid fibre; bending; yield band; yield stress; failure mechanism; kink)

INTRODUCTION

Oriented fibre-reinforced composites are used as high performance structural materials because of their high strength to density ratio. The mechanical behaviour is normally characterized using tensile, compressive and bending tests. Continuous fibre-reinforced composites are often subjected to bending loading rather than axial loading; hence, testing in bending is highly desirable as a means of characterizing the materials.

In bending, half of the beam is subjected to compression while the other half is under tension, and if the beam is elastic, the maximum tensile and compressive stresses are equal in magnitude. Consequently, bending failure of composites may occur due to tensile or compressive stresses. In composites reinforced with aramid fibres bending failure originates on the compression side of the beam[1] due to the lower compressive strength of the composite compared to its tensile strength.

Under compression, composites reinforced with aramid Kevlar-49 or SVM fibres (the properties of which are similar to Kevlar-49) fail with the formation of kinks[2]. Initially, in the 1970s, it was assumed that the compressive failure (kinking) of composites reinforced with aramid and other fibres was caused by fibre buckling similar to that of a beam on an elastic foundation[3]. However, now it is accepted that kinks in composites reinforced with aramid fibres are caused by compressive failure of the fibres[1,4,5], and that failure is not related to fibre buckling. Indeed, fibre buckling does occur if the matrix is insufficiently stiff to support the fibres, e.g. if the temperature is higher than the glass transition temperature of the epoxy matrix[1,6] or if a polyurethane matrix is used. The fibre buckling failure mode has two distinctive features: (1) the compressive strength is approximately equal to the shear modulus of the composite; and (2) the failure band is perpendicular to the fibre direction[1,6]. Absence of these features is an indication of some competitive failure mode, usually caused by failure of the fibres or by splitting of the matrix.

The goal of this work is to study the bending failure mechanism of a unidirectional aramid SVM/epoxy composite, and specifically to determine the angle between the yield bands and the loading direction.

MATERIALS

A unidirectional aramid SVM fibre-reinforced composite was used for this study. For reinforcement, 530 denier SVM yarns were used. The yarn comprised 300 fibres of 13 μm diameter. The matrix was a hot-curing epoxy EDT-10 composition, similar to DGEBA, consisting of 80% by weight of epoxy ED-20 resin (4,4′-diglycidylbisphenol A), 10% of diethylene glycol modifier and 10% of triethanolamine titanate curing agent.

Ring specimens were made by wet winding four parallel SVM yarns preimpregnated with liquid resin on to a cylindrical mandrel, 150 mm in diameter. The matrix was cured at 160°C for 4 h. The resulting rings were 8.4 mm thick, their width was 9.9 mm and the inner diameter was 150 mm. Interlaminar cracks or cavities were not noticed after curing of the matrix. Each ring was cut into

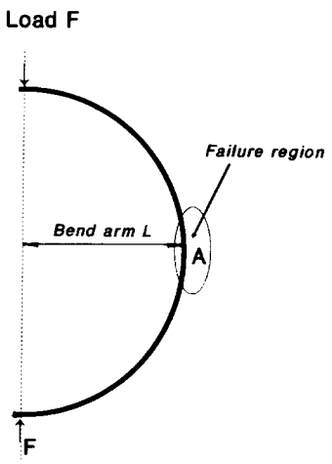

Figure 1 Schematic of two-point bending test

two half-rings. The fibre content of the composite was calculated from the cross-section of the ring specimen and the number of rotations of the mandrel during the winding process as 62% by volume.

TWO-POINT BENDING

Usually bending properties are determined in a three- or four-point bending test. A disadvantage of these tests is the concentration of stress under the loading points. To avoid stress concentration in a failure area, half-ring specimens were tested as shown in *Figure 1*. The bending moment is maximum near point A in the figure. Assuming a linear elastic response of the composite, bending stresses on the inner and the outer sides of the ring are given by[7]:

$$\sigma = \frac{Mq}{2I} \tag{1}$$

where: $M = FL$ is the applied bending moment; F is the load; L is the bending force arm; q is the thickness; and $I = wq^3/12$ is the second moment of the area of the beam cross-section about the axis of bending; and w is the width of the ring.

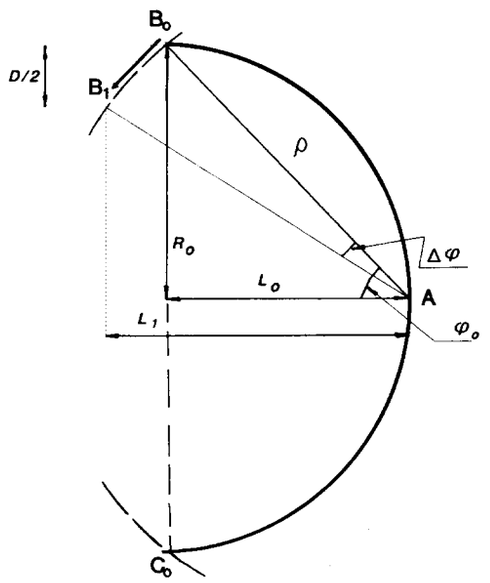

Figure 2 Plastic deformation of half-ring specimen. Yielding is supposed to be localized at point A

If the deformation of the specimen is very small, the increase in the bending arm L during testing may be neglected. However, in this work inelastic yielding of the composite was studied when half-rings were severely deformed, and in this case the change in L should be taken into account.

The bending arm can be determined as a function of the displacement of loading points as follows. Assuming that the yielding of the composite is localized near point A in *Figure 2*, the deformation is described by the rotation of two elastic beams about point A, where the composite behaves like a plastic hinge. During the test the load points B_0 and C_0 move along the dashed segment of the circle, centre A (*Figure 2*). The grip displacement D is equal to the difference between the initial and final distances between points B_0 and C_0. When the loading point B_0 shifts to point B_1, the grip displacement is given by:

$$D = 2\rho(\sin \varphi_0 - \sin \varphi_1) \tag{2}$$

where: φ_0 is the initial angle between point B_0 and the axis perpendicular to the loading direction (L in *Figure 2*); φ_1 relates to point B_1; $\rho = \sqrt{R_0^2 + L_0^2}$ is the radius of rotation; and L_0 is the initial bending arm.

Taking the difference of sine functions in equation (2) and assuming that the angular increment $\Delta\varphi = \varphi_0 - \varphi_1$ is small ($\Delta\varphi << 1$), so that $\sin \Delta\varphi = \Delta\varphi$ and $\cos \Delta\varphi = 1$, D is given by:

$$D = 2L_0\Delta\varphi \tag{3}$$

Similarly, the bending arm L_1 for point B_1 is given by:

$$L_1 = \rho \cos \varphi_1 \tag{4}$$

Combining equations (3) and (4) and taking into account that $\varphi_1 = \varphi_0 - \Delta\varphi$, the linear relation between the bending arm and displacement of the loading point is:

$$L_1 = L_0 + \frac{R_0}{2L_0} D \tag{5}$$

On the basis of equation (5), the bending arm was determined from the following half-empirical linear equation:

$$L_1 = L_0 + AD \tag{6}$$

where the coefficient $A = 0.48$ is a constant that was determined in preliminary experiments. This value is close to the theoretical estimate of 0.606 calculated with equation (5) for $R_0 = 79.2$ mm and $L_0 = 65.3$ mm.

All mechanical tests were conducted with an Instron model 1169 universal testing machine at a loading rate of 2 mm min^{-1}. The radii of the upper and lower loading points were 3.5 mm. In total, six half-ring specimens were tested. After mechanical testing the specimens were examined with optical and scanning electron microscopy (SEM). The angles between the yield bands and the fibre direction were measured with a low-magnification optical microscope with an angular error of 3'.

ORIENTATION OF YIELD PLANE

To determine the orientation of a yield plane in the case of three-dimensional yielding, the angle between the yield band and the loading direction must be determined in two planes. This can be done for yield lines intersecting the side edges of the specimen, as shown in *Figure 3*. The total angle Ψ between the yield plane and the loading direction was calculated using the equation derived in the Appendix:

$$\tan^2\Psi = \tan^2\Psi_1 + \tan^2\Psi_2 \qquad (7)$$

where Ψ_1 and Ψ_2 are the angles between the yield band and the loading direction on the compression and side surfaces of the half-ring.

RESULTS

Figure 4 shows a typical bending load *versus* displacement curve for the aramid SVM/epoxy composite. The curve is typical of the loading of ductile materials. At the point 1 several yield lines were distinctly observed on the inner compression surface. After this point, the load increases and then decreases smoothly with increasing displacement. The number and in particular the brightness of the yield lines gradually increased with loading. Arrow 3 shows the onset of fibre fracture on the outer tensile surface of the ring. Up to point 3 no peaks were visible on the curve, and the failure process was completely stable.

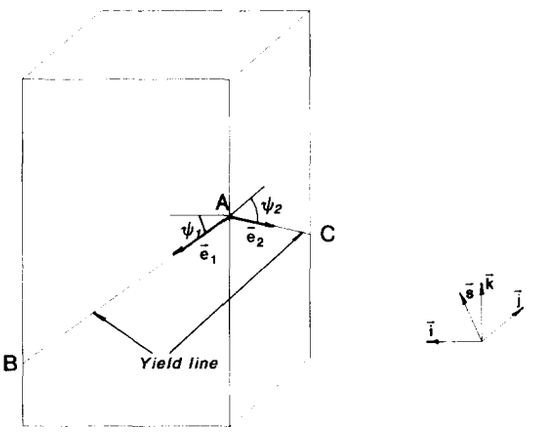

Figure 3 ABC yield plane. Ψ_1 and Ψ_2 are the angles of yield line orientation in the compression and side planes, $\vec{s}$ is the unity vector perpendicular to the yield plane and $\vec{i}$, $\vec{j}$ and $\vec{k}$ are unity vectors of the coordinate system

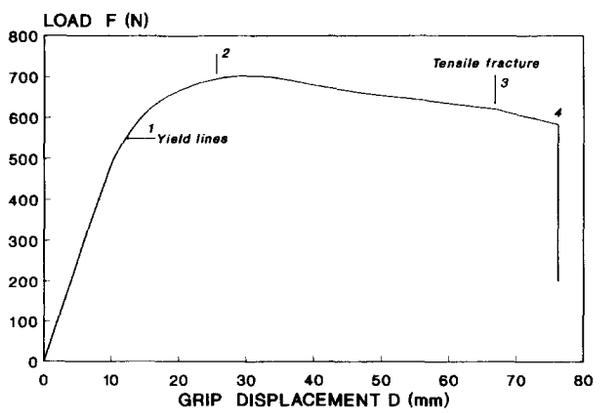

Figure 4 Load F plotted against grip displacement D

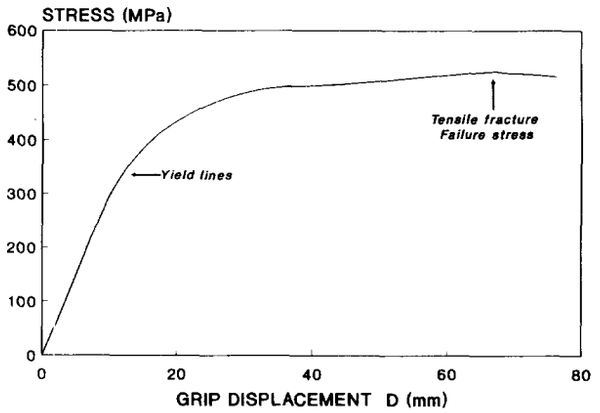

Figure 5 Bending stress plotted against grip displacement D

Figure 5 shows the stress–displacement curve calculated using equations (1) and (6). The curve is linear up to a stress of 300 MPa. The yield lines were noticed at a stress of 340 MPa, which is close to the composite strength under pure axial compression (260–280 MPa[1]). The maximum failure stress of 530 MPa is reached at the point where fibre fracture on the tensile surface was registered. The bending stress increased up to this point. Thus, although the cause of bending failure is compressive yielding of the composite, the reason for the decrease in bending stress is tensile fracture of the fibres. The maximum bending stress of 530 MPa is approximately two times higher than the strength of the SVM/epoxy composite under pure compression.

The yield bands were noticed at a stress of 340 MPa. From this value the yield stress of the fibres may be calculated, assuming that the yield stress of the composite is described by the rule of mixtures:

$$\sigma_c = V_f\sigma_f + V_m\sigma_m \qquad (8)$$

where: σ_m is the yield stress of the epoxy matrix; σ_f is the yield stress of the fibres; and V_f and V_m are the volume fractions of the fibres and the matrix.

For V_f = 62% and σ_m = 85 MPa[1], the yield stress of the fibres σ_f is calculated to be 500 MPa. This is an upper estimation of the fibre strength because the first yield bands might remain unnoticed. This value is close to the fibre strength in uniform compression, 400–450 MPa[1].

Figure 6 illustrates schematically the three regions of composite deformation under bending loading. In the first region (I) deformation of the composite is elastic. Failure processes start in the region II with the appearance of yield bands on the compression surface of the beam. Deformation leads to thickening and growth of the yield bands toward the tensile surface of the specimen. The final stage of failure, region III, consists of fracture of fibres in the tensile surface of the beam.

YIELD LINES

A photograph of the compression surface of the segment cut from the half-ring is shown in *Figure 7*. The specimen was unloaded at point 2 in *Figure 4*. A network of

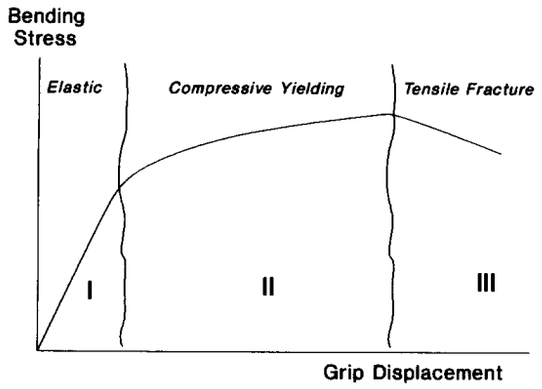

Figure 6 Schematic illustrating three stages of composite deformation

white intersecting lines that are almost perpendicular to each other and look similar to yield lines in ductile polymers is observed in the photograph. The yield bands are not straight and differ in brightness and thickness. Thick light lines parallel to the longitudinal direction of the specimen are due to different yarns.

Figure 8a shows the compression surface of the specimen loaded to higher deformation (point 4 in *Figure 4*). Three thick intersecting kinks and several thin yield lines are observed in the photograph. The specimen is severely deformed, and its width in the kinked region is 15% higher than the initial width. *Figure 8b* shows the side view of the same specimen, with kinks propagating through 75 to 80% of the total beam thickness. The yield lines, especially the thick ones, in *Figure 8b* are not perpendicular to each other. Hence, the angle of yielding changes during testing.

ORIENTATION OF YIELD PLANE

The orientation of the yield lines was determined for the initial stage of yielding, between points 1 and 2 in *Figure 4*. Some yield lines in *Figure 7* are perpendicular. Hence, these bands are oriented at an angle of 45° to the loading direction. However, lines that are not perpendicular to each other are also observed. To determine the orientation of the yield plane, the angle between the yield line and the fibre direction was determined in two perpendicular planes, on the compressive and side surfaces of the specimen. After this the angle Ψ was calculated from equation (7).

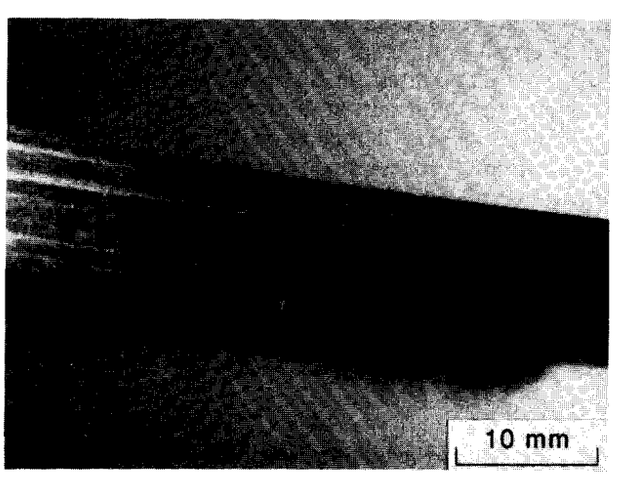

Figure 7 Photograph of compression surface. The specimen was unloaded at point 2 in *Figure 4*

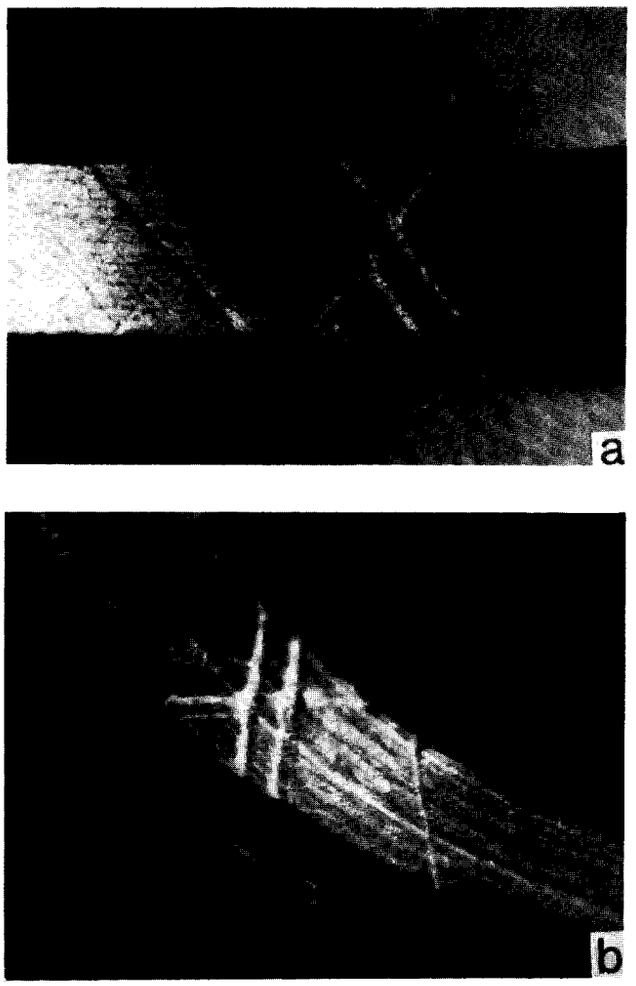

Figure 8 Specimen loaded to higher deformation (up to point 4 in *Figure 4*): (a) top and (b) side views

The results for 15 yield lines intersecting the side edge of the beam are presented in *Table 1*. Although the average angle $\langle\Psi_1\rangle$ (*Figure 3*) in the compression plane is 41.5°, the total angle $\langle\Psi\rangle$ between the yield planes and the fibre direction is 44.8±1.7°. Thus, the yield lines are initiated almost exactly at an angle of 45° to the loading direction, i.e. in the plane of maximum shear stress. Hence, bending failure of the aramid/epoxy composite is

Table 1 Bend angles

Line number	Ψ_1 (°)	Ψ_2 (°)	Ψ (°)
1	43.8	10	44.2
2	38.5	30	44.5
3	39.2	31	45.3
4	43.4	14	44.3
5	42.3	11.5	43
6	42.2	28.3	46.5
7	43.1	28	47.1
8	40	22.1	43
9	38.5	25	42.7
10	41.3	18.5	43.2
11	44	14.5	45
12	45	8	45.3
13	44	13	44.8
14	38	40.8	49.3
15	38.4	25.5	42.8
Average	41.5	21.3	44.8±1.7

caused by shear yielding in the compression part of the beam, similar to slip yielding in ductile metals. The composite is a highly anisotropic material. Despite this, it yields in the plane of maximum shear stress, as does an isotropic material. This is an unexpected result. It means that the orientation of the fibres does not change the direction of yielding.

The experimental inaccuracy in Ψ values was ~1° for each band. This is caused by the curvature of the bands and, additionally, by the limited length of the bands on the side surface of the half-rings. The scatter in the average $\langle\Psi\rangle$ value for 15 yield bands is 1.7°.

MICROSCOPY

Figure 9 shows a photograph of the compression surface of the specimen obtained in the dark field of a reflective optical microscope. The specimen is the same as that in *Figure 7*. The microscope was focussed on a plane below the surface level. Several white yield bands are observed on the photograph. The specimen surface is not plane, and hence the whole area is not completely in focus.

At higher magnification, the yield bands (see *Figure 10*) show thin yield lines and arrowed V- and N-bands in single fibres, and comparatively thick yield bands. The angle between the lines in the V-bands is 52–60°. The boundaries of the yield bands in *Figures 9* and *10* are often relatively sharp and bounded by comparatively bright yield lines. Note that either comparatively thin microyield lines in single fibres or yield bands thicker than 7–10 μm are observed. The absence of yield bands of intermediate thickness (1–7 μm) may be explained by the formation of an N-band in a fibre. The appearance of a V-band represents a turn in the fibre at one point (*Figure 11*), and a kink, that is a double turn in opposite directions, may be represented by an N-band, as shown schematically in *Figure 11*.

Figure 12a shows an SEM micrograph of the inner compression surface of the same specimen. In the centre of the photograph the yield band can be observed. The fibres in the yield band are tilted so that a kink is formed. The matrix in the band is cracked, thus facilitating observation of the kink. The angle between the initial fibre direction and the orientation in the kink is estimated at 30–40°. *Figure 12b* shows an SEM micrograph of a kink that is approximately four times thicker than the kink in *Figure 12a*. The angle of fibre tilting is 32–38°, and hence the structure of the kink is similar to that in *Figure 12a*. Thus, after a kink is formed, further yielding consists of self-similar growth of the kink. Short yield lines in single fibres were not observed with SEM. SEM gives a surface image and yielding is not registered until the matrix is cracked in a kink. In contrast, optical microscopy may be focussed below the surface, thus allowing observation of yield lines, even if a kink is not formed.

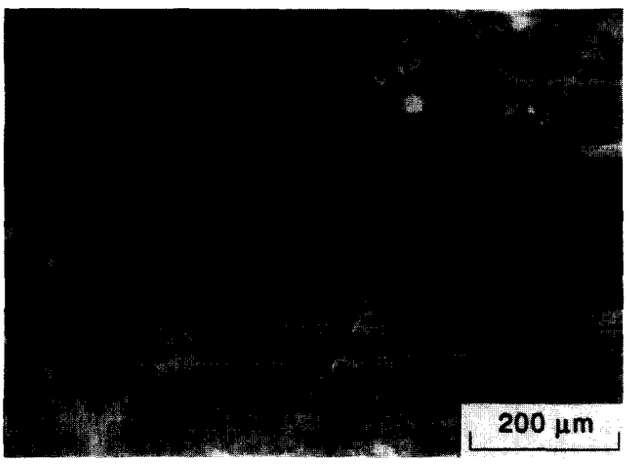

Figure 9 Dark field reflective optical micrograph of compression surface of specimen shown in *Figure 7*

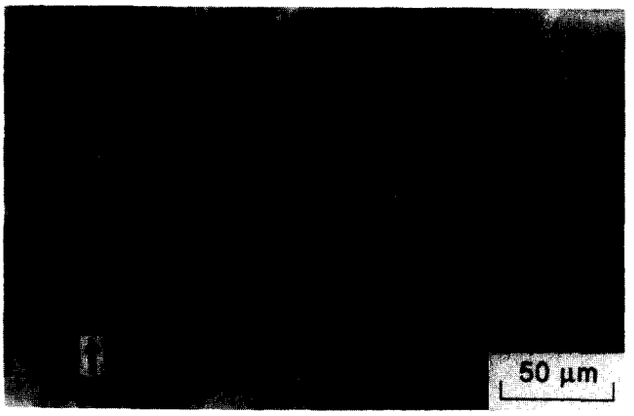

Figure 10 Higher magnification of compression surface

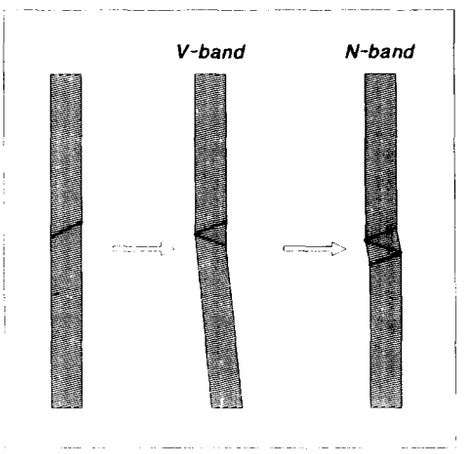

Figure 11 Schematic of formation of a kink

THICKENING OF YIELD BANDS

Figure 13 schematically illustrates the yield band oriented at an angle of $\Psi = 45°$ to the loading direction. The fibres in the yield band are not broken, which leads to thickening of yield bands.

Figure 14 shows the local thickness of yield bands T plotted against shear displacement of the fibres in a perpendicular direction S. The dependence is described by a straight line, except for the initial part of the curve corresponding to the formation of a kink. The slope of the straight line a log–log plot is equal to 1. This indicates that kink thickness increases proportional to the shear displacement S. This conclusion is confirmed by *Figure 15* which shows the ratio of the thickness to shear displacement T/S plotted against S. At $S > 6$ μm

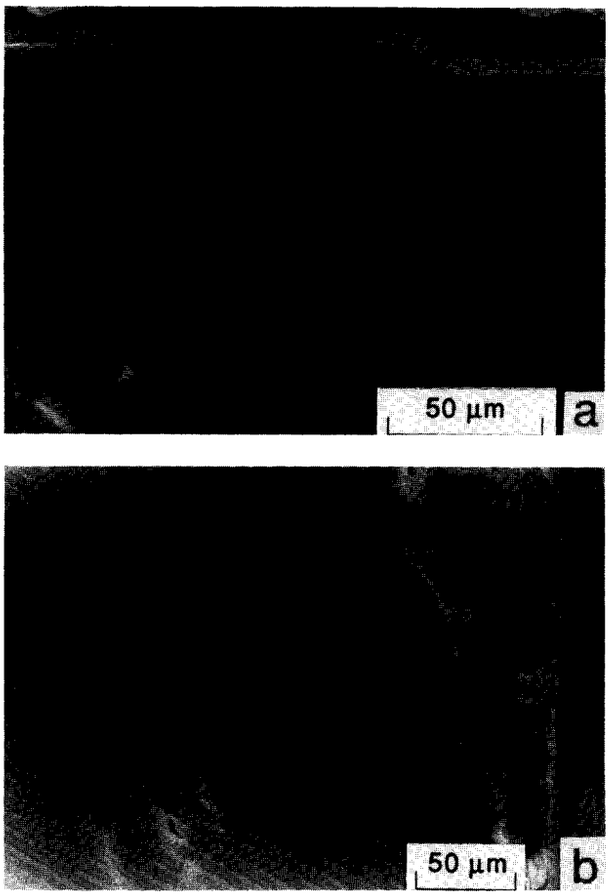

Figure 12 SEM micrographs of two kinks with different thicknesses

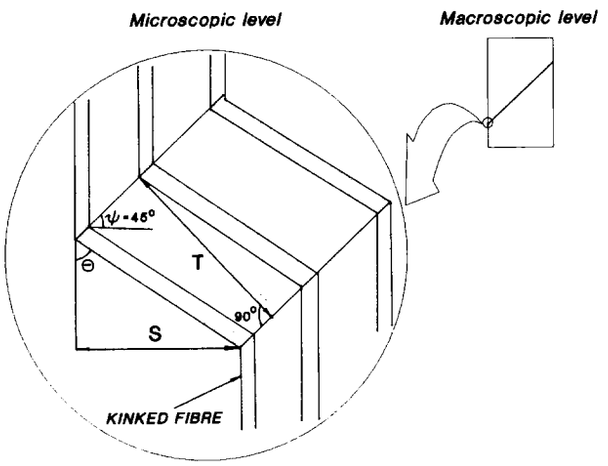

Figure 13 Schematic of a yield band (θ = angle of fibre tilting in the kink)

and $T > 12$ μm the ratio is practically constant and T is given by:

$$T = AS \tag{9}$$

where A is 1.8 ± 0.2. Thus, shear deformation leads to a proportional thickening of the yield bands. On the initial region of the curve in *Figure 15* the T/S ratio decreases with an increase in shear deformation S.

If fibres in the kink are tilted at an angle θ to their direction as shown in *Figure 13*, the relation between T, S and θ is:

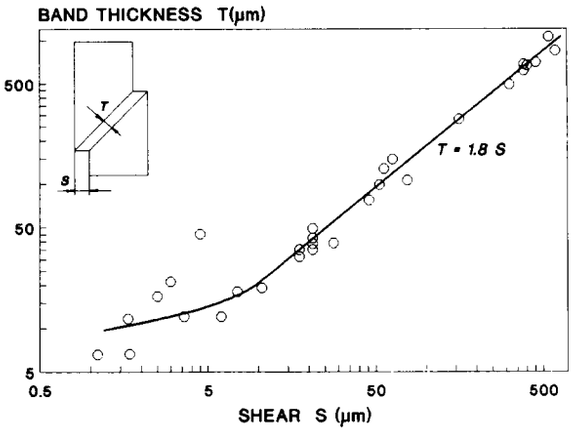

Figure 14 Thickness of yield bands T plotted against fibre displacement S

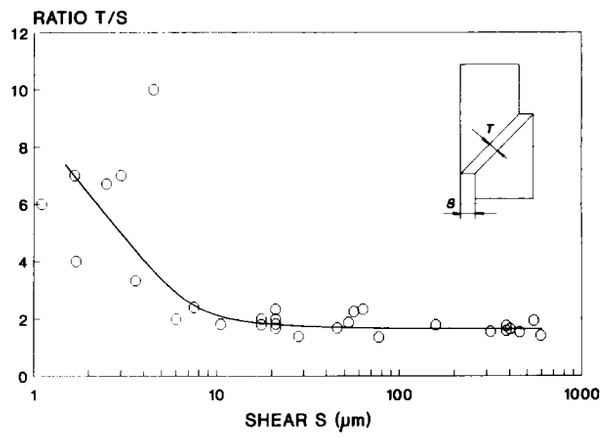

Figure 15 Ratio of kink thickness to fibre displacement T/S plotted against fibre displacement S

$$T = \frac{\cos(\pi/4 - \theta)}{\sin \theta} S \tag{10}$$

This equation explains the proportionality between T and S if the angle θ remains unchanged. Hence in this region yielding consists of the growth of a self-similar kink. The coefficient of proportionality is equal to $\cos(\pi/4 - \theta)/\sin \theta$. For $\theta = 32$–$38°$ this coefficient varies from 1.84 to 1.61. This value is close to the experimental value of 1.6–2. The decrease in the T/S ratio in *Figure 15* corresponds to an increase in angle θ during deformation, i.e. to tilting of the fibres in the kink. The decrease in the T/S ratio confirms that the kink is not formed by continuous thickening of a thin microyield line in a fibre, and that there is a stage of kink formation.

Figure 16 summarizes the results of optical and SEM studies of the yield bands, and illustrates schematically the possible yield mechanism of the composite. Failure is originated by compressive yielding of a single fibre (a) followed by the formation of a yield N-band in the fibre (b). Further shear leads to an increase in the angle of fibre tilting in the yield band, so that a kink is formed (c). At this stage of yielding, the ratio of kink thickness to shear decreases. The next yield step is the growth of a self-similar kink (d), where the T/S ratio remains constant.

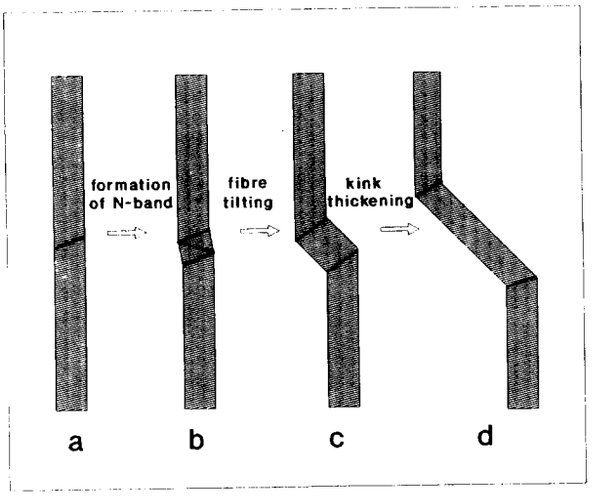

Figure 16 Schematic of yield mechanism

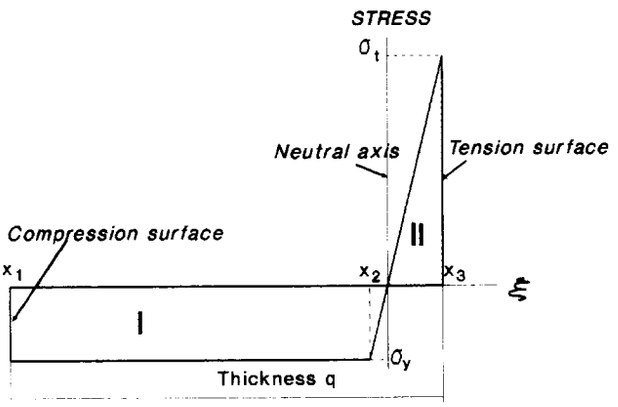

Figure 17 Distribution of bending stress over thickness of beam. σ_y is the yield stress in compression and σ_t the maximum tensile stress

RELATION BETWEEN BENDING AND COMPRESSIVE YIELD STRENGTHS

It is generally assumed that the composite fails if a critical tensile, compressive or shear stress is reached, and furthermore these critical values coincide with the strengths determined from uniform stress tests. However, the bending strength of the composite is approximately twice as great as the compressive strength. This may be explained by stable growth of kinks toward the tensile part of the beam with increasing load.

After the maximum failure bending load is determined, it can be substituted in an appropriate equation, e.g. equation (1), assuming a linear elastic response of the beam. However, this assumption for the aramid/epoxy composite was not fulfilled in practice. Hence to determine failure stress, plasticity theory must be used. Plasticity theory has been developed for isotropic metals where the yield stress in tension is equal to that in compression. The bending failure stress for an isotropic rigid-plastic material is one and a half times higher than the yield stress[7].

To find the relation between the maximum (failure) stress in bending and the yield stress in compression, plasticity theory was extended to the aramid/epoxy composite. The composite was assumed to be homogeneous, elastic in tension and elastic-plastic in compression. The bending stress distribution σ for this case is described in *Figure 17*. The neutral plane where axial stresses are equal to zero is shifted toward the tensile surface. Using classical bending theory of an isotropic beam, applied to an anisotropic material, the bending moment per unit width is found by integration of the product $\sigma\zeta$ over the thickness of the beam:

$$M = \int_{x_1}^{x_3} \sigma(\zeta)\zeta \, d\zeta \tag{11}$$

where $\sigma(\zeta)$ is the distribution of the axial stress over the beam thickness and ζ is the distance from the neutral plane. Integration of equation (11) for the stress distribution shown in *Figure 16* gives:

$$M = \sigma_y(x_1^2/2 - x_2^2/6) + \sigma_t x_3^2/3 \tag{12}$$

where: x_1 is the distance from the neutral axis to the compression surface; x_2 is the distance to the yield zone; x_3 is the distance to the tension surface; σ_y is the yield stress in compression; and σ_t is the stress at the outer tensile surface.

The total axial load in bending is equal to zero. Hence, the area of compression (region I) in *Figure 17* is equal to the area of the region in tension (II):

$$x_1\sigma_y - x_2\sigma_y/2 = x_3\sigma_t/2 \tag{13}$$

The compressive yield stress σ_y and tensile stress σ_t in *Figure 17* are related to the following equation:

$$\sigma_t/x_3 = \sigma_y/x_2 \tag{14}$$

and the total thickness of the beam is given by:

$$x_1 + x_3 = q \tag{15}$$

Solution of equations (13)–(15) gives:

$$x_3 = \frac{\sigma_y}{\sigma_t/2 + \sigma_y + \sigma_y^2/2\sigma_t} q \tag{16}$$

and

$$M = \frac{\sigma_y(q - x_3)^2}{2} + \frac{\sigma_t x_3^2}{3} - \frac{\sigma_y^3 x_3^2}{6\sigma_t^2} \tag{17}$$

where q is the thickness of the specimen. Assuming that the yield stress in compression is negligible in comparison with the tensile stress σ_t ($\sigma_y \ll \sigma_t$), equation (16) gives $x_3 = 0$. Substituting $x_3 = 0$ into equation (17), the bending moment is given by:

$$M = \sigma_y q^2/2 \tag{18}$$

If the stress distribution is elastic, the bending moment

is given by[7]:

$$M_o = \sigma_y q^2 / 6 \qquad (19)$$

If $\sigma_y \ll \sigma_t$, the maximum bending moment for a ductile material in compression and an elastic material in tension [equation (18)] is three times higher than M_o for an elastic material [equation (19)]. Hence, the bending strength calculated from equation (1) is three times higher than the compressive yield stress.

The beam fails when the tensile stress σ_t reaches the magnitude of the composite tensile strength σ^*. *Figure 18* shows M/M_o plotted against the ratio of the composite tensile strength to compressive yield stress σ^*/σ_y, as calculated from equations (16) and (17). If $\sigma^* = \sigma_y$ the bending failure stress is equal to σ_y. Increase in σ^*/σ_y results in a growth of bending strength, that finally asymptotically approaches the triple compressive yield stress. For the SVM/epoxy composite, $\sigma^* = 2.5$ GPa and $\sigma_y = 260$ MPa, and hence $M = 2.6\ M_o$. This explains why the bending strength of the composite is higher than the compressive yield strength. The theoretical estimation of $x_3 = 0.17q$ is close to the experimental value of $x_3 = 0.2$–$0.25q$.

DISCUSSION

In bending, the failure of the aramid SVM fibre-reinforced composite is caused by shear yielding of the composite near the compression surface. First yield bands are oriented exactly at $\Psi = 45°$ to the compression direction. Hence, compressive failure in bending is caused by shear yielding of the composite, and kinks are analogous to slip bands in metals. A similar 'shear' failure mechanism of carbon fibre-reinforced composites in compression was proposed by Evins[8], by DeFerran and Harris[9], and by Sierakowski with co-workers[10].

Shear yield in oriented polymers has some specific features that are not observed in metals. Atoms in metals after experiencing shear on their periodicity length 'forget' about their initial position. In contrast, in polymers molecular chains are not broken, and this leads to kinking which is sometimes mistaken for buckling. Unbroken molecular chains also lead to characteristic thickening of the yield bands with deformation. The mechanism of yield thickening in oriented polymers, caused by unbroken molecules, differs from that in metals.

In pure axial compression the kink angle is 48–52° to the compression direction[1]. It was noticed that in bending, thick kinks deviated from a 45° angle and hence the angle between the loading direction and the kink plane increases a little with yielding. This may be the cause of some difference of the angles in bending and in axial compression, when failure instability does not allow observation of the initial yield stages, and the kink thickness is never less than 40–60 μm.

The ductility of the SVM/epoxy composite in compression and elasticity in tension is a unique feature that is not observed in other materials. As a result, yielding of the composite in bending is not described by classi-cal plasticity theory developed for isotropic materials.

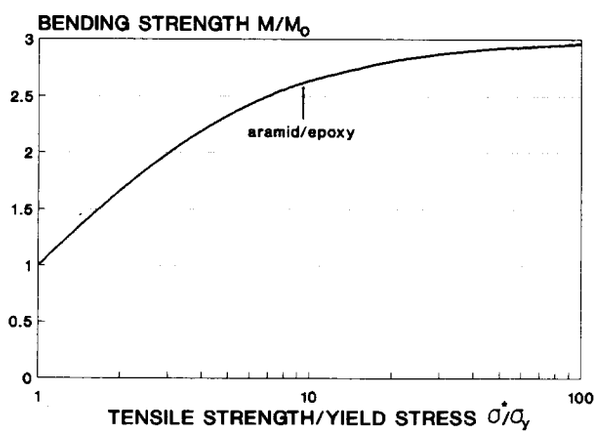

Figure 18 Bending failure moment M/M_o plotted against ratio of composite tensile strength to compressive yield stress σ^*/σ_y

CONCLUSIONS

1) Flexural failure of a unidirectional aramid SVM/epoxy composite originated near the compression surface of the beam. The final stage of the failure process is fracture of fibres near the opposite tensile surface of the beam.
2) Compressive failure is caused by shear yielding of the composite, similar to yield in shear bands in metals.
3) In bending the first yield bands are oriented at an angle of $45 \pm 2°$ to the fibre direction.
4) The thickness of yield bands (kinks) increases proportionally to the local shear displacement of the opposite side of the band.
5) Failure stress in bending is approximately twice as high as the yield stress of the composite in pure compression.
6) In bending the composite is elastic in the tensile part of the beam and elastic-plastic in the compression part.

ACKNOWLEDGEMENTS

The author is grateful to Professor L.I. Manevich for stimulating discussions and to Drs A.M. Kuperman and A.Ya. Gorenberg for technical help.

REFERENCES

1 Bazhenov, S.L., Kozey, V.V. and Berlin, A.A. *J. Mater. Sci.* 1989, **24**, 4509
2 Hahn, H.T. in 'Proc. 6th Int. Conf. on Composite Materials', Vol. 1 (Eds F.L. Matthews, N.C.R. Buskell, J.M. Hodgkinson and J. Morton), Elsevier Applied Science, London, 1987, p. 269
3 Rosen, B., Kulkarney, C. and McLaflin, P. in 'Inelastic Properties of Composite Materials' (Ed. K. Herakovich), Mir, Moscow, 1978, p. 33 (in Russian)
4 Deteresa, S.J., Allen, S.R., Farris, R.J. and Porter, R.S. *J. Mater. Sci.* 1984, **19**, 57
5 Yeh, J.R. and Teply, J.L. *J. Compos. Mater.* 1988, **22**, 245
6 Bazhenov, S.L. and Kozey, V.V. *J. Mater. Sci.* 1991, **26**, 6764
7 Kachanov, L.M. 'Plasticity Theory', Nauka, Moscow, 1969
8 Evins, P.D., *Technical Report N-70007*, Royal Aircraft Establishment, Farnborough, UK, 1970
9 DeFerran, E.M. and Harris, B. *J. Compos. Mater.* 1970, **4**, 62
10 Sierakowski, R.L., Newill, G.E., Ross, C.A. and Jones, E.R. *J. Compos. Mater.* 1971, **5**, 362

APPENDIX

To determine the orientation of the yield plane, the three-dimensional yielding in *Figure 3* is considered. If vectors of the coordinate system are $\vec{i}$, $\vec{j}$, and $\vec{k}$, the unity vector perpendicular to the yield plane $\vec{s}$ may be written as:

$$\vec{s} = a_1\vec{i} + a_2\vec{j} + a_3\vec{k} \tag{A1}$$

where a_1, a_2 and a_3 are coefficients. The length of the $\vec{s}$ vector is equal to one:

$$a_1^2 + a_2^2 + a_3^2 = 1 \tag{A2}$$

The angle between the unity vector oriented along line AB in *Figure 3*, $\vec{e}_1$, and the $\vec{i}$ vector is Ψ_1, and hence $\vec{e}_1$ is given by:

$$\vec{e}_1 = \cos\Psi_1\vec{i} + \sin\Psi_1\vec{k} \tag{A3}$$

Similarly, the unity vector along line AC in the side surface is given by:

$$\vec{e}_2 = \cos\Psi_2\vec{j} + \sin\Psi_2\vec{k} \tag{A4}$$

Vectors $\vec{e}_1$ and $\vec{e}_2$ are in the yield plane and hence the scalar products $(\vec{s}, \vec{e}_1)$ and $(\vec{s}, \vec{e}_2)$ are equal to zero:

$$a_1\cos\Psi_1 + a_3\sin\Psi_1 = 0 \tag{A5}$$

$$a_2\cos\Psi_2 + a_3\sin\Psi_2 = 0 \tag{A6}$$

The cosine of the angle between the load direction $(\vec{k})$ and the $\vec{s}$ vector is given by:

$$\cos\Psi = (\vec{s}, \vec{k}) = a_3 \tag{A7}$$

The solution of equations (A2) and (A5)–(A7) is:

$$\cos^2\Psi = \frac{1}{1 + \tan^2\Psi_1 + \tan^2\Psi_2} \tag{A8}$$

Considering that $\sin^2\Psi = 1 - \cos^2\Psi$, and dividing $\sin^2\Psi$ by $\cos^2\Psi$, equation (7) is obtained.